MUTUAL ADJUSTMENT OF MASS FLUX AND STRATIFICATION PROFILES

BRIAN E. MAPES
CIRES, University of Colorado
Boulder, Colorado, 80309-0449 USA

Abstract

Observations indicate that deep convective heating profiles tend to oppose temperature perturbations in the environment. As a result, convection adjusts the stratification toward a preferred moist adiabat. A buoyancy-sorting model of precipitating convection, coupled with a linearized hydrostatic dry dynamics model, illustrates the processes at work. The preferred stratification established by the model convection depends on the treatment of precipitation and ice processes, and especially on the poorly-understood processes that determine mass flux in downdrafts associated with the evaporation of precipitation. These results suggest that observations of mean stratification in convecting regions may contain useful, highly averaged information on hard-to-observe bulk parameters characterizing the ensemble of real convective clouds. Temperature perturbations of < 1 C are quite important in this buoyancy-sorting model, suggesting that such stratification observations should be scrutinized to this precision.

1. Introduction

The sensitivity of convective entrainment and detrainment to environmental stratification has been discussed by Haman (1969), Raymond and Wilkening (1982), Bretherton and Smolarkiewicz (1989), Ferrier and Houze (1989), Taylor and Baker (1991), and Mapes and Houze (1995), among others. It is found that convective clouds tend to eject mass laterally into particularly strongly stratified layers of their environment. Thus, penetrating convective clouds can be visualized as prising apart isentropes wherever they are pressed together, and pressing them together where they are far apart (at least in the perturbation sense). This is equivalent to saying that convection heats the environment more where is it anomalously cool, and heats less where the environment is anomalously warm.

As a result, convection tends to adjust the environmental density profile toward some preferred mean state. What aspects of the convection determine this state? Can sounding observations be used to deduce, or at least tune, the bulk parameters representing the ensemble of convective cloud systems?

Section 2 mathematically defines the relationships between profiles of vertical mass flux, horizontal wind divergence, and convective heating rate. Section 3 summarizes Mapes and Houze's (1995) divergence observations, and the associated deductions from a thermally-forced model. Section 4 describes the results of coupling a simple buoyancy-sorting model of convection with a linear model of the stratified dynamics of its surroundings.

2. Vertical mass flux, horizontal divergence, and heating

2.1. THE BASIC IDEA, IN WORDS

Convection transfers mass vertically among layers in a stratified atmosphere. Precipitating convection in particular effects a net upward cross-isentropic flow of mass. Low-entropy air from low levels is deposited in higher-entropy layers aloft, the additional entropy being created primarily by the release of latent heat of condensation. The net mass sink in low layers draws in mass from surrounding regions, while the mass source aloft causes a diverging motion that spreads the added mass over a large region. This convergence of mass at low levels and divergence of mass at upper levels in response to convective heating occurs rapidly, as a gravity wave process, with characteristic velocity up to 50 m/s. As a result, the latent heat released in a precipitating convective cloud is quickly spread over a large area, causing only slight temperature perturbations at any point. More detail on this process is given in section 4.

The cross-isentropic flow - that is, the heating of the atmosphere by convection - can therefore be characterized by the mass sink or source (divergence of the horizontal wind) as a function of potential temperature. If the temperature response of the atmosphere to localized heating events is rapid and efficient, then the basic atmospheric stratification may change very little during a convective event. In this case, profiles of horizontal wind divergence as a function of height (from radar data), or of pressure (from radiosonde data), contain the signal of the heating of the atmosphere by convection.

2.2. MATHEMATICAL DEFINITIONS

2.2.1. *Diabatic divergence*

The linearized thermodynamic equation in pressure coordinates is:

$$C_p \frac{dT}{dt} + \omega\sigma = Q \tag{1}$$

where C_p is heat capacity, T is temperature, ω is vertical velocity (g x mass flux), σ is a static stability parameter, and Q is heating rate. This equation can be solved for ω:

$$\omega = \frac{Q}{\sigma} - \frac{C_p \frac{dT}{dt}}{\sigma} \equiv \omega_d + \omega_a \tag{2}$$

which defines the diabatic vertical velocity ω_d as heating rate divided by static stability. We define the diabatic divergence δ_d as the partial derivative of ω_d with respect to pressure. Physically, the diabatic divergence is that profile of horizontal divergence which prevents temperature from changing in the presence of a localized internal atmospheric heating Q(p). In practice, because heating rates are so much greater than temperature

changes inside a mesoscale convective system, the total divergence (as in Fig. 1) is, within measurement errors, equal to the diabatic divergence: $\delta \sim \delta_{d.}$

The utility of interpreting a divergence profile as a diabatic divergence profile is that it can be used to specify the heating in a primitive equation model of thermally forced circulations. First, δ_d can be spectrally decomposed in terms of the vertical "modes" of a linearized primitive equation model of the atmosphere. We have calculated these modes for realistic stratification, using the vertical transform code of Fulton and Schubert (1985). In the linear approximation, each mode evolves independently, as waves propagating on the specified fixed stratification. Solutions to the 3-dimensional primitive equations, subject to the specified thermal forcing, can be obtained by superposition of these vertical modes. Each mode (mode index n) satisfies the barotropic divergent flow (shallow water) equations, characterized by a nondispersive wave speed c_n. For each mode, the thermal forcing is specified as the corresponding coefficient δ_{dn} in the spectral expansion of the diabatic divergence $\delta_{d.}$

The divergence theorem expresses how area-integrated divergence can be accurately and easily estimated from measurements of the line-normal horizontal velocity component along a line bounding the area in question:

$$\iint_A \delta dA = \oint_{perim} \vec{V}_h \bullet d\hat{n} \tag{3}$$

3. Observations of horizontal divergence

The perimeter integral in the divergence theorem can be evaluated using Doppler radar, which gives a good estimate of one component of the horizontal wind (the along-beam component), at any point where precipitation hydrometeors exist in sufficient quantity. If the sampling geometry is such that this along-beam wind component is the component normal to a closed curve, then summing the velocity around the curve gives area-integrated divergence. MH95 performed this integration of airborne Doppler radar data around 146 circular regions of 30-60 km diameter inside ten diverse tropical mesoscale convective systems. The result was 146 area-average divergence profiles (the integration was performed at different altitudes, for 500 m layers of the atmosphere).

For present purposes let us just examine the grand mean of all 146 profiles (Fig. 1). The profile is characterized by convergence below 9km, and divergence above. Extrema of both mean convergence and its standard deviation occur just at and above the melting level (4.7km). The profile is not mass balanced, because radar does not adequately sample the intense divergence in the highest reaches of the upper troposphere. Furthermore, the surface value is subject to large error because of sea clutter interfering with the radar measurements. But because divergence profile measurements extend through most of the troposphere, the spectral decomposition of the mean profile is not too sensitive to details of how the profile is completed at the top and bottom.

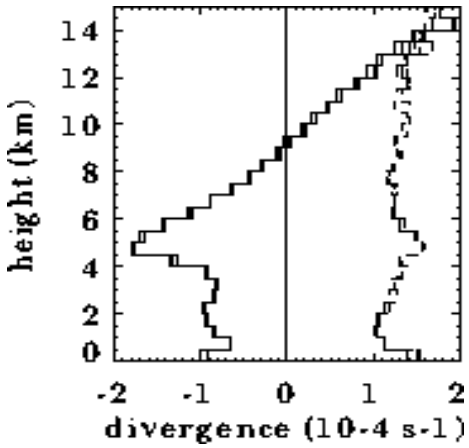

Figure 1. The mean of all 146 divergence profiles within 10 MCSs (solid) and the standard deviation of the sample at each level (dash).

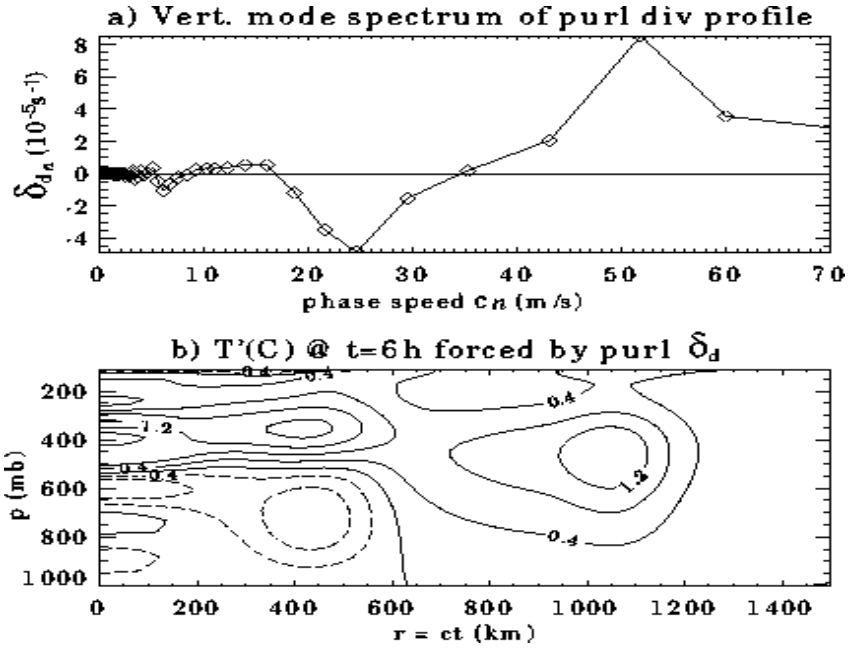

Figure 2. a) The spectral transform of the divergence profile of Fig. 1, in terms of the vertical modes of a realistically stratified linear primitive equation model. b) The temperature change in a linear resting model, caused by a 140 km radius region of heating

with the profile of Fig. 1&2a. The heating was switched on 6h before the time of the temperature field contoured here and maintained thereafter.

The spectral transform of the MH95 mean divergence profile of Fig. 1 reveals a remarkable spectral simplicity (Fig. 2a). To illustrate the meaning of the spectral expansion, Fig. 2b shows the temperature anomaly field, constructed by the modal superposition procedure described above, as a function of radius from a mesoscale (140 km) cylindrically symmetric region of heating whose δ_d profile is that indicated in Fig. 1. In this case, the imposed heating was switched on 6h before the time of Fig. 2b, in a nonrotating resting atmosphere. Associated with each of the main spectral bands in Fig. 2a is a temperature signal, the faster phase speeds c being associated with deeper vertical structures.

Three main features are seen in Fig. 2: a single-signed warming of the whole troposphere, associated with a phase speed c ~ 50 m/s; a two-signed temperature structure with c ~ 25 m/s; and a high-wavenumber signal with c ~ 6 m/s. There is a remarkable lack of amplitude at low c, aside from the c ~ 6 m/s signal, which is associated with the melting of snow at the 550-600 mb level. Furthermore, this melting signal is spectrally localized, and therefore spatially extended: the temperature signal associated with this melting feature is a wavelike pattern of temperature anomalies spanning the depth of the troposphere. How can we understand such observations?

4. Interaction of ambient temperature and convective heating

That convective heating reacts to ambient temperature anomalies was apparent in MH's divergence observations of one particular mesoscale convective system on Feb 6, 1993. These observations are summarized in the schematic Fig. 3, which indicates the observed divergence anomalies (horizontal arrows) associated with a cool temperature anomaly at low levels in the environment of this one particular MCS (dashed contours). Extra convergence below the cool layer, and extra divergence above it, were observed - 'extra' compared to the other cases in the data set.

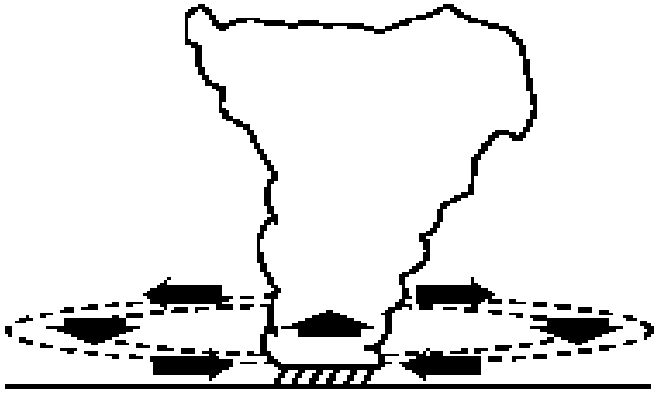

Figure 3. Schematic of observations of Feb 6 MCS, with cool anomaly (dashed) and divergence anomalies (horizontal arrows).

These observation show the essence of the buoyancy interactions between convection and its environment. The in-cloud mass flux is anomalously upward within the cool layer (upward fat arrow). This extra mass flux is consistent with the fact that any air in the cloud, whether positively buoyant updraft or negatively buoyant downdraft, feels extra buoyancy within this layer. Whether the extra mass flux reflects increased updraft mass flux or decreased downdraft mass flux cannot be determined from these observations. In any case, the extra upward net mass flux implies extra net condensation, and hence extra convective heating, which is expressed in the environment as extra subsidence (downward arrows). Note that this extra heating in the cool layer tends to oppose the temperature anomaly that created it.

Can this mechanism explain the spectral simplicity of the mean profile? Because each convective cell in an MCS occurs in the wake of many previous cells, it "feels" the residuum of high vertical wavenumber temperature perturbations left by previous convective cells (and any other diabatic processes). Suppose a convective cell in an MCS undergoes some random, sharp entrainment or detrainment process that causes a high vertical wavenumber (low c) δ_d signal. This heating causes a temperature perturbation which, because of the low value of c, is essentially locally trapped. The next (or adjacent) convective cell will then tend preferentially to damp the temperature perturbation, as in Fig. 3. As a result, the average δ_d over many cells will tend to be free of any systematic high wavenumber (low c) components. The wavelike " melting reverberation" pattern is an exception, because it is continuously forced.

5. Modeling interacting convective heating & temperature

To illustrate these processes in action, let us take a model of convection that responds to environmental temperature in the manner outlined above, i.e. with heating that opposes temperature anomalies. Almost every convective cloud model and parameterization does so, although different physical explanations are associated with this mechanism in different schemes. Naturally, convection schemes that adjust the temperature toward some moist adiabat or other reference profile will oppose anomalies of all kinds. A more physically enlightening model is that of Raymond and Blyth (1989, 1992, hereafter RB).

5.1. THE RAYMOND-BLYTH BUOYANCY-SORTING MODEL

The RB model is based on the concept of buoyancy sorting. A convective cloud is idealized as an updraft parcel of air from low levels which ascends to its highest level of neutral buoyancy along some kind of moist adiabat. At each intervening level in the atmosphere, 9 mixing events are assumed to take place, creating mixtures of ambient and updraft air. These mixtures span the range of mixing fractions from 0.1 to 0.9. Each of these mixed "sub-parcels" is then assumed to ascend or descend (based on its buoyancy) to its nearest level of neutral buoyancy. The result is that, from an input sounding and input parcel, the RB model predicts a profile of the detrainment of neutrally buoyant air. Since the entrainment profile is also known (equal masses of ambient air come from all

levels through which the cloud penetrates), the RB model essentially predicts a δ_d profile, given a sounding.

Suppose we replace the specified mesoscale heating at the center of Fig. 2b with the more interactive RB model. The RB model predicts the time-evolving δ_d profile based on the time-evolving temperature field in the convective region, while the linearized primitive equations predict temperature perturbations, based on the time history of δ_d. The interactions discussed above should be evident in this model. Of course, we still have to specify the magnitude of the convective heating; the RB model just gives the profile. We also specify the initial sounding (here a mean of >2000 tropical west Pacific soundings from TOGA COARE).

The buoyancy profile of a parcel traversing a precipitating moist adiabat from the boundary layer of the mean COARE sounding is shown in Fig. 4a and c. In Fig. 4a, the moist adiabat is defined without freezing effects. Precipitation is crudely parameterized by allowing the parcel to carry a maximum of 3 g/kg of suspended condensate. The buoyancy (including water vapor and liquid contributions to density, but expressed as degrees C) is negative below ~800 mb and is about 2C through the 600-200 mb layer. When the water that condenses above the 0C level is allowed to freeze, the parcel experiences extra buoyancy, to a maximum of 4C at 250 mb. The suspended condensate carried across the 0C level is not allowed to freeze; if it did, the sudden release of latent heat would give the parcel even more buoyancy.

The resulting δ_d profiles returned by the RB model are shown in Fig. 4 b,d,f. To mass balance these profiles, the boundary-layer air assumed to constitute the core of the updraft is indicated as a strong convergence in the lowest 60 mb. A downdraft parameterization is essential to counteract the extremely unrealistic effects of this concentrated convergence (see below). When freezing is neglected (Fig. 1b), the model detrains significant amounts of mass at middle levels as well as near the top of the troposphere. This may not be too unrealistic in some situations; in nature, the freezing process does not necessarily occur at 0C, as is assumed in equilibrium thermodynamics, and thin midlevel layer clouds are indeed frequently observed in convective regions of the tropics. However, for convection growing in the wake of previous convection inside an MCS, it is difficult to justify exclusion or even delay of freezing. When freezing is included (Fig. 4d), the midlevel detrainment is significantly less.

Figure 4f shows the divergence profile after a simple downdraft parameterization is included. The strong convergence at the surface is substantially cancelled by the downdraft's divergence, while midlevel convergence into downdraft changes the sign of the total divergence through much of the troposphere. This profile is much more realistic, but notice the high wavenumber feature, with convergence at 600 mb and divergence at 750 mb. This feature arises from the mean stratification at those levels, as discussed below.

The downdraft parameterization assumes that 40% of precipitation evaporates during fallout. The profile of this evaporation was calculated from the temperature dependence given by Eq. (7.17) of Rogers and Yau (1989). In doing so, we have assumed that the drop size distribution of precipitation (assumed to be liquid) is constant with height,

as is the relative humidity of the air through which it falls. In nature, the humidity of the air through which the precipitation particles actually fall depends on the fine-scale space and time geometry of the convective cloud and its neighbors, and on the aerodynamics of rainshaft downdrafts themselves, as well as on “ambient” humidity, wind shear, etc. This is a formidable problem, so only a crude treatment is warranted in a simple model.

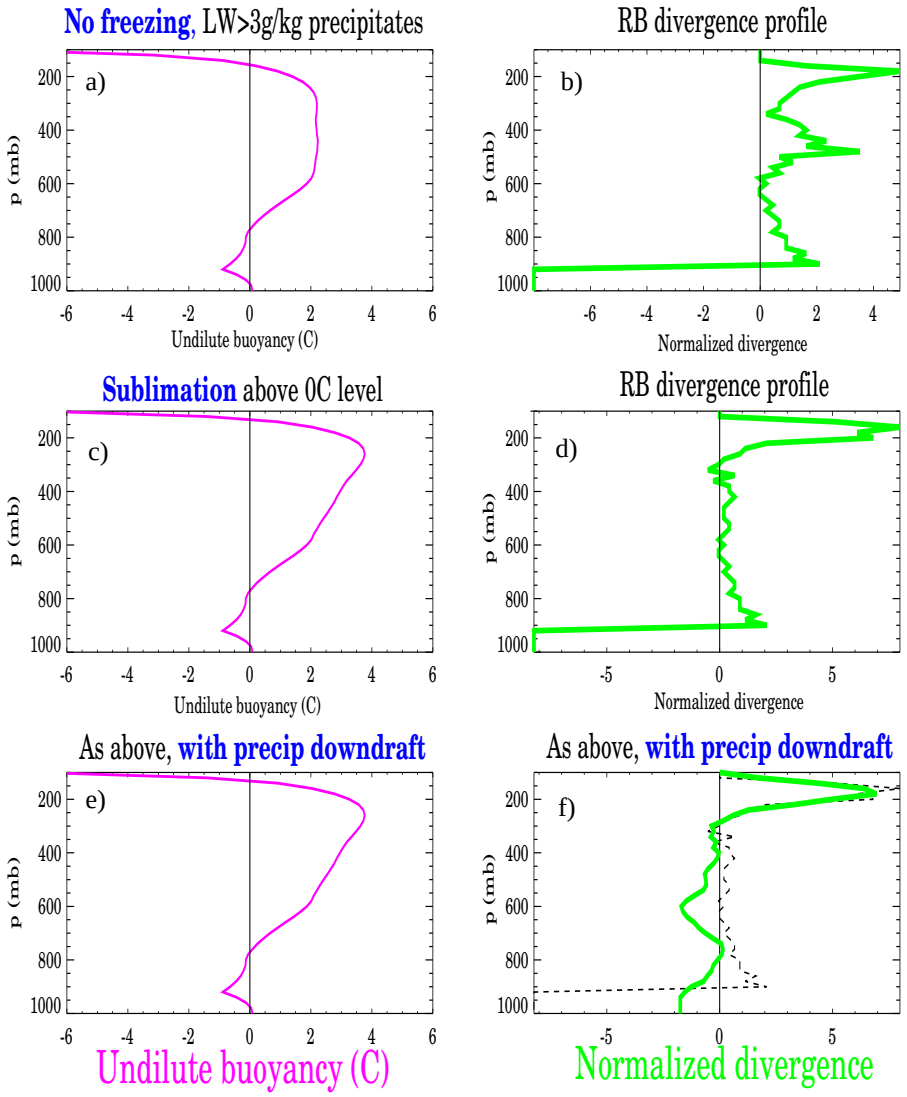

Figure 4. The Raymond-Blyth model’s responses to the COARE mean sounding. Left column: undilute parcel buoyancies for different assumptions about ice and precipitation. Right column: the corresponding divergence profiles.

The resulting evaporation profile decreases monotonically with height from the surface, becoming very small above the 350-400 mb level. Evaporation was converted to a diabatic mass flux according to (2), and thence to a diabatic divergence. This δ_d profile contains a high-wavenumber 'kink' at 600 - 750 mb, owing to a fluctuation of the static stability σ at those levels in the observed mean sounding [see (1)]. An important thing to note is that this downdraft δ_d profile is essentially noninteractive: its sensitivity to small environmental temperature perturbations is extremely weak, because the mean static stability is always used in calculating δ_d in this linearized model. This downdraft also has no sensitivity to the environmental humidity profile.

5.2. THE RB+DOWNDRAFT CONVECTION'S PREFERRED STRATIFICATION

The temperature perturbation field after 6 hours of heating, with the profile given by the interactive RB+downdraft model, is shown in Fig. 5. The heating profile was updated every 20 minutes, based on the model's response to the evolving temperature field in the heated zone, a Gaussian function of radius extending to r=200 km. As in Fig. 2b, we see a troposphere-deep wave of warming that has affected a large area, out to r = 1200 km. At smaller radii, a number of higher-wavenumber structures are evident.

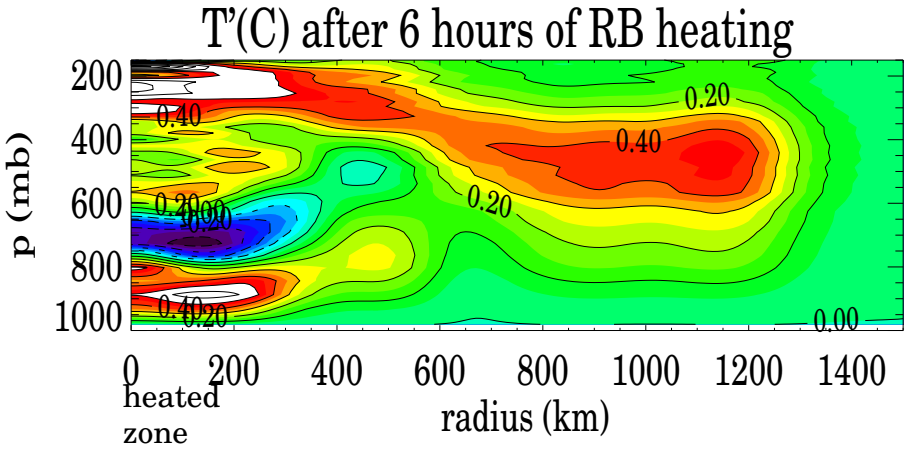

Figure 5. The temperature perturbation field after 6 hours of model convection, with specified intensity but interactively determined profile (c.f. Fig 2b).

Most notable among them is the high wavenumber temperature structure at low levels, excited by the downdraft parameterization's structure (Fig. 4f). The buoyancy-sorting effects of the RB model updraft oppose the growth of this temperature anomaly, by the mechanism indicated in Fig. 3. As a result, the temperature structure attains a moderate intensity, at which the heating and cooling processes balance. In circular geometry there is no steady equilibrium: eventually T' at small radius goes to 0, as gravity-wave processes spread the added heat over an area proportional to the square of time. For this high wavenumber, though, this dynamic spreading is relatively slow (Fig. 5). For a field of heat sources, or in slab geometry, a steady equilibrium would result, with a permanent

temperature structure like that near the origin in Fig. 5. In this equilibrium, the noninteractive downdraft's high-wavenumber kink in δ_d (Fig. 4f) is balanced by an opposite kink that develops in the RB updraft's interactive δ_d profile.

In short, the RB + downdraft cloud model simply has an equilibrium stratification that differs from the observed COARE mean stratification, in the way indicated by the T' profile in and near the heated zone in Fig. 5. The buoyancy profile of the convecting parcel in this new stratification is plotted in Fig. 6 (dashed line). The differences (< 1 C) are not very large compared to the mean buoyancy. Nonetheless, they are large enough to significantly alter the model convection's heating profile, i.e. to make the updraft compensate for the shortcomings of the downdraft parameterization. Note also that the negative buoyancy experienced by the parcel at low levels increases significantly, because we specified a heating rate independent of this 'negative area.' Real convection might shut itself off if it created such a warm layer at low levels.

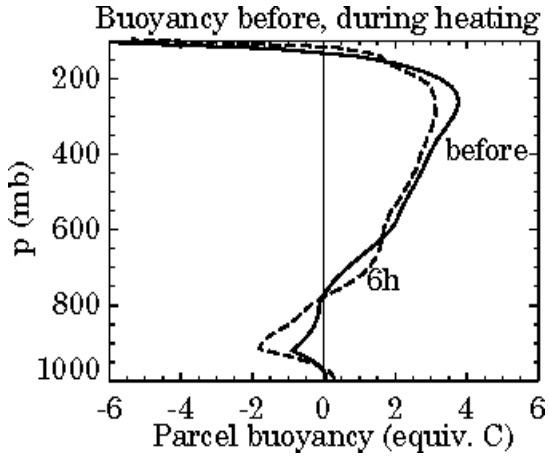

Figure 6. Buoyancy profiles of an undilute precipitating parcel in the COARE mean sounding (solid), and after 6h of the RB+downdraft cloud model heating (dash).

This raises an important question: what kind of updraft and downdraft dynamics, what forms of precipitation, freezing, and rain evaporation, determine the mean stratification profile in nature? One way to tune the present convection model toward these natural values would be to adjust its parameters such that it gives a divergence profile as much like the observed mean (Fig. 1) as possible, when it is given the observed mean sounding as an input. The first place for improvement would be with the crudely specified downdraft. Such an exercise is beyond the scope of this small study, but should be part of the development of cumulus parameterization schemes intended for prediction.

5.3. SENSITIVITY STUDIES

Although this model simulates poorly the mean mass flux profile, given observed mean stratification (Fig. 4f), and hence simulates the mean stratification poorly when allowed

to feed back on itself (Fig. 5-6), its sensitivity is illustrative. Suppose, for example, that we tell the convection there is a cool anomaly in the 500-600 mb layer, Gaussian in profile, with a -1C peak value. The time-evolving and 6h time-mean response of the Raymond-Blythe divergence profiles to this temperature anomaly are shown in Fig. 7. Extra mass detrains above the cool anomaly, while less mass detrains below, exactly as in the schematic Fig. 3.

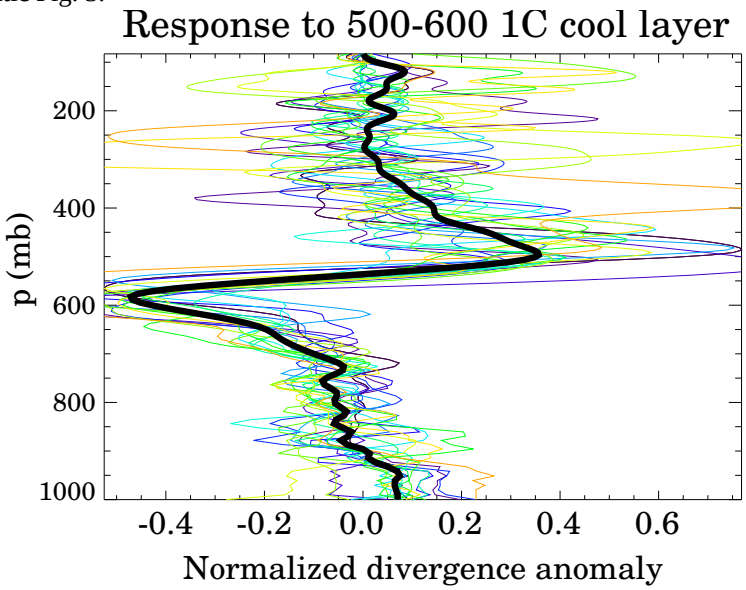

Figure 7. The anomalous divergence response of the RB cloud model, every 20 minutes for 6 hours (light lines) and mean (heavy line), to a 1C Gaussian cool anomaly in the 500-600 mb layer.

The resulting heating anomaly warms the layer, opposing the T anomaly (Fig. 8):

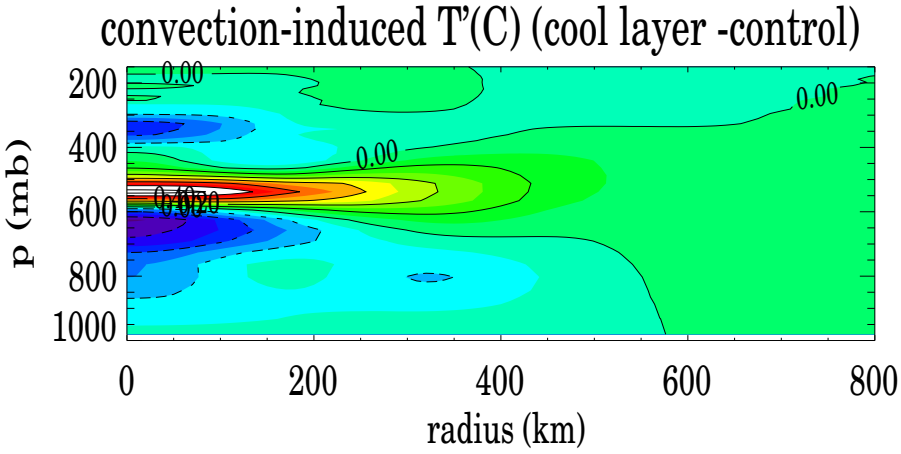

Figure 8. Temperature anomaly caused by the anomalous divergence profiles of Fig. 7

Now suppose instead that we continuously cool the same layer, in analogy to the continuous melting of snow. Fig. 9 shows the radial wind perturbation (essentially, the time-averaged δ_d perturbation) delivered by the RB model when exposed to this "melting," and its direct effects. A multilayered perturbation wind structure, reminiscent of the melting "reverberation" seen near the origin in Fig. 2, is indicated. Of course, in nature we observe some combination of the direct effects of melting and the convection's response, so the connection of Fig. 9 to observations is not entirely clear.

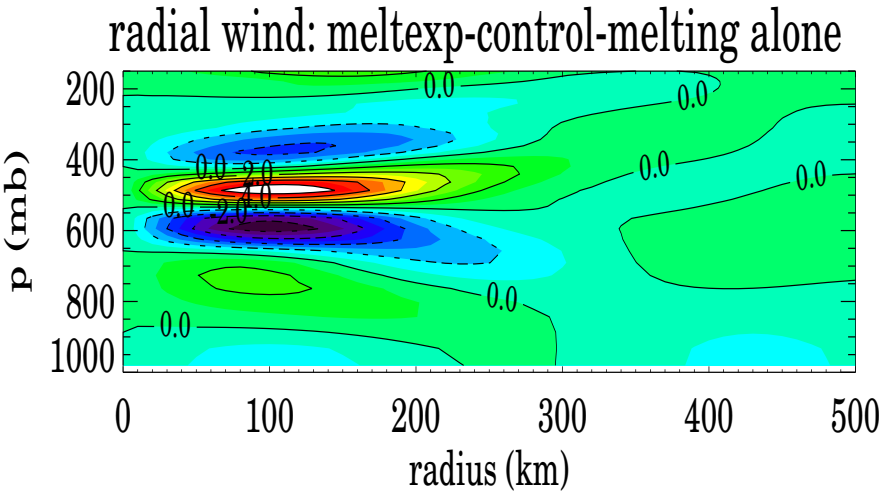

Figure 9. The radial (divergent) wind anomaly developed by the model convection as a response to a steady cooling applied continuously in the 500-600 mb layer in the convective zone (0-200 km radius).

6. Conclusions

Vertical mass flux in deep convective clouds interacts with the environmental stratification. In particular, convective heating opposes temperature profile anomalies, tending to adjust the stratification toward its preferred version of a moist adiabat. The particular nature of that moist adiabat is determined by the bulk properties of updrafts (including the microphysics of freezing and precipitation within them), and of downdrafts driven by the evaporation of precipitation. Much can be learned about the bulk, mean properties of real atmospheric convection from a close study of observed stratification profiles. Tools like the RB model used here, but with more realistic and interactive models for downdrafts, entrainment, etc., might be used to retrieve the bulk parameters governing real convection, from observed soundings in regions whose stratification is primarily determined by ubiquitous deep convection (e.g. in the tropics over wam seas).

Buoyancy changes of ~1C can be quite important to convection, so temperature anomalies of this magnitude, whether in models or observations, must be taken seriously.

References

Bretherton, C.S., and P.K. Smolarkiewicz, 1989: Gravity waves, compensating subsidence, and detrainment and detrainment around cumulus clouds. *J. Atmos. Sci*., **46**, 740-759.

Ferrier, B.S., and R.A. Houze, Jr., 1989: One-dimensional time-dependent modeling of GATE cumulonimbus convection. *J. Atmos. Sci.*, **46**, 330-352.

Fulton, S.R., and W.H. Schubert, 1985: Vertical normal mode transforms: theory and application. *Mon. Wea. Rev.*, **113**, 647-658.

Haman, K., 1969: On the influence of convective clouds on the large-scale stratification. *Tellus*, **XXI**, 40-53.

Mapes, B.E., and R.A. Houze, Jr., 1995: Diabatic divergence profiles in west Pacific mesoscale convective systems. *J. Atmos. Sci.*, **52**, 1807-1828.

Raymond, D.J., and A. M. Blyth, 1986: Extension of the stochastic mixing model to cumulonimbus clouds. *J. Atmos. Sci.*, **49**, 1968-1983.

Raymond, D.J., and M.H. Wilkening, 1982: Flow and mixing in New Mexico mountain cumuli. *J. Atmos. Sci.*, **39**, 2211-2228.

Taylor, G.R., and M.B. Baker, 1991: Entrainment and detrainment in cumulus clouds. *J. Atmos. Sci.*, **48**, 112-121.

Acknowledgment

This research was supported by a TOGA-COARE grant, jointly funded by the U.S. NOAA Office of Global Programs (OGP) and the U.S. National Science Foundation, administered by NOAA OGP. David Raymond kindly provided the code on which this buoyancy sorting cloud model was based. Mark DeMaria provided the Fulton and Schubert vertical transform code. Careful review of this manuscript by Roger Smith resulted in significant clarifications.